applied sciences

MDPI

Article

A Stay Cable Icing Identification Method Based on the Fusion of U-Net and ResNet50

Zhiyong Yang, Feng Xiong, Yaoyao Pei, Zhi Chen *, Chuanhai Zhan, Enjie Hu and Guanghao Zhang

School of Civil Architecture and Environment, Hubei University of Technology, Wuhan 430070, China; yzy621@163.com (Z.Y.); 13308687680@163.com (F.X.); yaoyao.bae@foxmail.com (Y.P.); zhanchuanhai1999@163.com (C.Z.); 13103929130@163.com (E.H.); 17762509225@163.com (G.Z.)
* Correspondence: chenzhi1988420@126.com

Abstract: The identification of stay cable icing is crucial for robot deicing to improve efficiency and prevent damage to stay cables. Therefore, it is significant to identify the areas and degree of icing in the images of stay cables. This study proposed a two-stage model that combines U-Net and ResNet50. In the first stage, this model used U-Net to segment the surface ice and icicles from the stay cable. The image of icing obtained after segmentation was used as the input for the second stage. In the second stage, ResNet50 was used to classify the degree of icing. The experimental results show that the proposed model can successfully segment the icicles and surface ice from the stay cable icing image to complete the classification of the icing degree. The mean pixel accuracy and intersection over the union of icing were 96.65% and 82.10%, respectively. The average accuracy of the icing degree classification was 95.71%. The method proposed in this study meets the requirements of robustness, segmentation accuracy, and classification accuracy for stay cable icing recognition, which provides a research basis for the precise icing recognition of cable-deicing robots.

Keywords: icing; fuses U-Net and ResNet50; two-stage model; icing degree classification

check for updates

Citation: Yang, Z.; Xiong, F.; Pei, Y.; Chen, Z.; Zhan, C.; Hu, E.; Zhang, G. A Stay Cable Icing Identification Method Based on the Fusion of U-Net and ResNet50. *Appl. Sci.* **2024**, *14*, 3062. https://doi.org/10.3390/app14073062

Academic Editor: Christos Bouras

Received: 18 January 2024
Revised: 26 February 2024
Accepted: 1 March 2024
Published: 5 April 2024

1. Introduction

An important structural component of cable-stayed bridges is the stay cables. The aerodynamic performance of the stay cable changes when the phenomenon of icing occurs on its surface, leading to relaxation phenomena [1]. As the ice melts, falling ice will threaten road traffic safety and cause long-term road congestion and bridge blockades [2], resulting in substantial economic losses and severe social impacts. Therefore, local municipal administration departments should clear the icing to address the security risks caused by cable icing.

At present, the artificial deicing of stay cables presents challenges such as long working cycles, high labor intensity, and poor safety, making it unsuitable for large cable-stayed bridges. As motor integration advances, the cable-deicing method using robots has received extensive attention and research [3]. However, the deicing robot is susceptible to external environmental factors, such as uneven distribution of cable icing, and the motor output may not match the load, leading to low deicing efficiency and even damage to the outer surface of the stay cable, thereby affecting the bridge's service life. Accurately recognizing the icing area and icing degree of stay cables is key to achieve high-precision deicing.

In recent periods, there has been increased research on ice-falling disasters of stay cables. Several scholars have studied bridge icing detection and prediction. An automatic detection method for bridge icing has been proposed [4]; this method uses weather data such as freezing rain, fog, and wet snow to predict bridge icing [5]. Bayes probability network was used to evaluate the probability of meteorological conditions and icing curves. [6] used the Fourier transform analysis model, the autoregressive model, and the continuous wavelet transform analysis to analyze ice thickness detection signals, and it was pointed out that the damage-sensitive features extracted by the two models were related to the icing phenomenon. Although the above methods recognize the icing state, the index will respond only when the icing thickness is large, and the icing state in front of the deicing robot cannot be reflected in real time.

With the advancement in computer vision and image recognition technology, image recognition based on deep learning has been applied in various detection fields, such as face recognition [7], transmission line icing detection [8], and biomedical image analysis [9,10]. Ref. [11] improved the accuracy of segmentation by introducing skip connections between encoder and decoder features, and this network is appropriately named U-Net and is used for segmenting neuron structures in the EM stack. Ref. [12] proposed the use of U-NET++ to evaluate pulmonary nodule segmentation, colonic polyp segmentation, nuclear segmentation, and liver segmentation. Ref. [13] proposed a hybrid deep convolutional neural network (CNN) model for the automatic and accurate prediction and segmentation of brain tumors from magnetic resonance imaging (MRI) images. These medical images have provided good segmentation results. Icing segmentation is similar to medical image segmentation; the pixels in the image are classified, so simple semantic segmentation is enough to deal with icing segmentation.

However, semantic segmentation alone can only identify the icing area without providing information on the icing degree. This lack of accurate classification data of the icing degree makes it challenging to control the motor output effectively for deicing. On the one hand, excessive output will cause excessive mechanical wear and energy waste. On the other hand, insufficient output will affect the deicing effect. Therefore, automatic classification of icing severity has become an urgent need. Image classification is the key to achieving the classification of icing severity. With the emergence of image classification networks such as CNN [14], image classification based on deep learning has gradually become a new research topic; CNN has a mature application in the field of icing identification.

Ref. [15] proposed a new critical point-matching method based on the local multi-layer CNN features, termed Local Convolutional Features (LCFs), to measure the ice thickness of the PTLI. Ref. [16] proposed an identification method for ice thickness based on a solid generalization convolution neural network (SGCNN), which is used to identify the thickness grade of the ice insulator of the transmission line. Ref. [8] used the lightweight convolutional neural network MobileNetV3 for feature extraction and the multi-scale target detection network SSD to extract high latitude features to achieve ice thickness recognition. The deep learning model has the potential for icing detection, so the image classification network can be used to identify the icing degree of stay cables. However, it is necessary to label the cable icing image before image classification. It is challenging to quantitatively evaluate the icing based on the complex icing growth characteristics [17]. A method should be proposed to quantify the classification of icing degree.

In recent years, much of the literature has adopted a two-stage deep learning method. Ref. [18] developed a two-stage deep learning method for missing electrical insulator string detection. In the first stage, the insulator string components in the detection area were segmented by semantic segmentation. In the second stage, the segmented mask was input into the CNN for detection to improve the model's accuracy. Ref. [19] adopted a two-stage deep learning method. In the first stage, DeepLabV3+ was used to segment the leaves from the background, and the image obtained after segmentation was used as the input for the second stage. In the second stage, U-Net was used to segment the diseased leaves. Finally, the ratio of the lesion's pixel area to the leaf's pixel area was calculated to classify the leaves.

The research on cucumber leaf disease segmentation and insulator string segmentation in complex backgrounds has progressed. However, there are few studies on cable icing detection in deep learning frameworks. Based on the existing research, this study proposes a two-stage cable icing detection model combining U-Net and ResNet50 [20] for specific angle cable icing images. The main contributions of this paper are as follows:

(1) A stay cable icing identification model with a two-stage architecture was proposed based on deep learning. This model achieved the accurate segmentation of the surface

ice and icicles and the classification of icing degree grade, which provided a basis for the precise deicing of the stay cable deicing robot.

(2) An icing degree grade classification method was proposed. The method calculates the mask area and uses it as a label to input into the classification network. Compared with the direct use of mask area to classify the icing level, this method improved the generalization ability [21].

(3) The cable icing data set was made, which makes up for the vacancy in this field.

The remaining structure of the paper is outlined as follows: Section 2 provides an overview of the establishment and preprocessing of the stay cable icing data set. Section 3 presents the framework for icing identification and quantification. Section 4 details the experimental procedures and examines the test results. Finally, Section 5 summarizes the new method and evaluates the feasibility of this study.

2. The Establishment of the Cable Icing Data Set

Deep learning heavily relies on abundant training data, often obtained from large public data sets. However, in the context of this study, there need to be more data sets that meet the needs of two-stage deep learning networks to address this need and to train and test the feasibility of our deep learning model. This chapter discusses the construction of a stay cable icing data set, which collects stay cable icing samples by simulating the perspective of a stay cable deicing robot. Based on the relatively tricky data acquisition on the cable-stayed bridge, samples were obtained through the stay cable icing experiment.

2.1. Experiment Preparation

2.1.1. Experimental Equipment

1. The step-in laboratory had constant humidity and temperature; the model was RH-60 (Andersen Instrument Equipment Co., Ltd., Wuhan, China), with an external size of 10 m × 5 m × 2.8 m and a temperature range of −60. The height of the rainfall device (Andersen Instrument Equipment Co., Ltd., Wuhan, China) was 2400 mm, the upper width was 2000 mm, and the three spray devices were evenly distributed. The spray flow range was 0~3 L/min, and the water temperature control range was 0.5~2 °C.
2. The camera fixed bracket (Made by a 3D printer Andersen Instrument Equipment Co., Ltd., Wuhan, China) simulated the perspective of the stay cable deicing robot, as shown in Figure 1. The size was 21 cm × 5 cm × 10 cm (diameter × thickness × length). The two cameras were connected by a 10 cm pole and the horizontal angle between the camera and the cable was set to 30°. Through two cameras, the degree of icing on one side of the stay cable can be judged separately, and the diversity of the data set can be increased.

Figure 1. Camera fixed bracket.

3. A practical engineering stay cable sheath with a diameter of 0.2 m, a wall thickness of 0.005 m, and a length of 2 m was used, and the sheath was smooth and hydrophobic.
4. Other equipment used in this experiment included a meteorological instrument (Beijing Sun Technology Co., Ltd., Wuhan, Chain), a cable-stayed bracket with adjustable

angle, a fan, two Hikvision network cameras (DS-IPC-B12V2-1) (HIKVISION Co., Ltd., Zhejiang, Chain), and an anemometer, as shown in Figure 2 (stay cable ice experimental equipment).

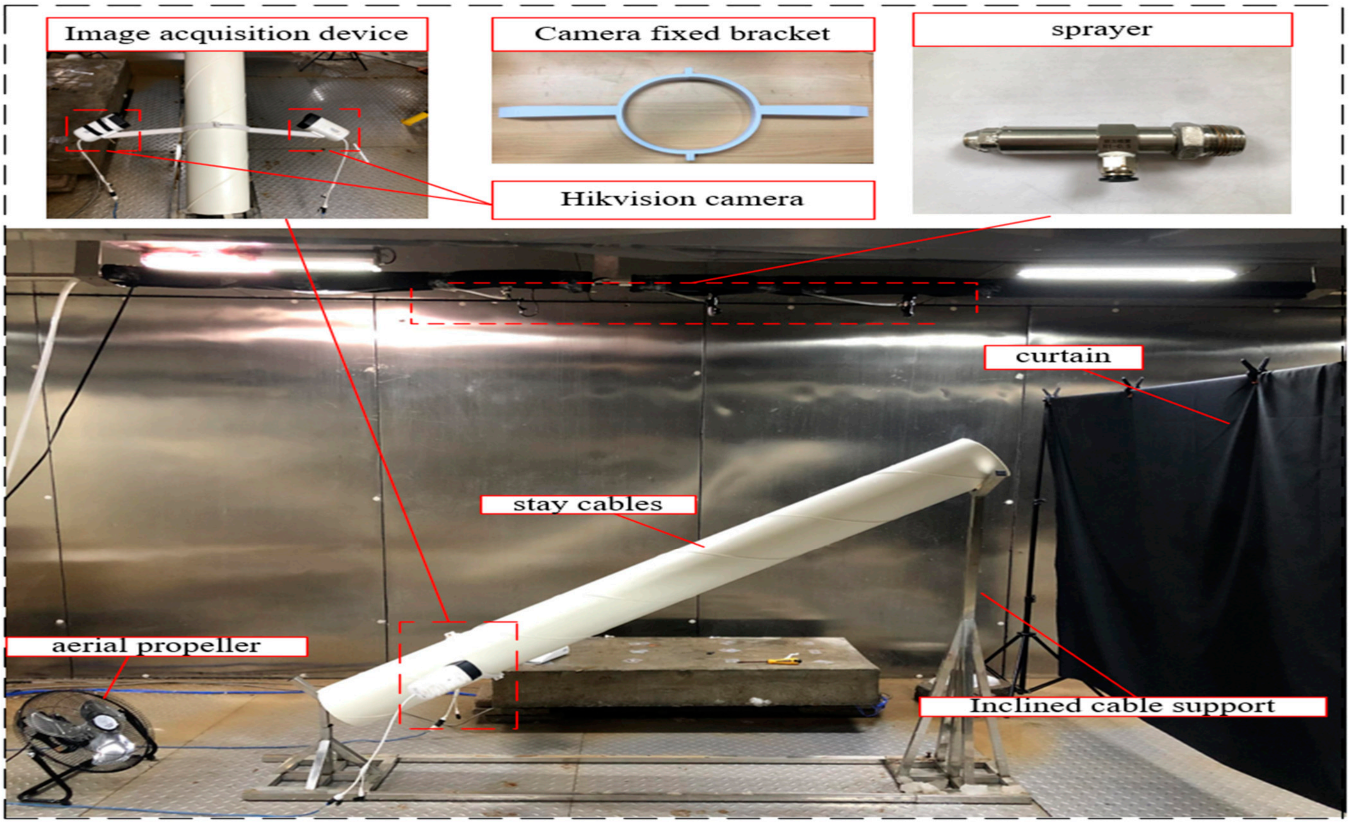

Figure 2. Stay cable ice experimental equipment.

2.1.2. Experimental Conditions of Stay Cable Icing

(1) Environmental temperature: The minimum temperature of Wuhan in the past five years was −8 °C, and the classic icing environment of the bridge is −4 °C. Therefore, this paper assumes that the ambient temperature is −8 °C and −4 °C.

(2) Wind speed: The dominant wind direction in winter is northwest wind. In this experiment, a fan was set in the direction the of northwest wind, and its wind speed was set to 2 m/s.

(3) Cooling time: This experiment selected the cooling time from 3:00 a.m. to 6:00 a.m. (3 h). After cooling, the indoor temperature was adjusted to 2 °C until the ice was completely melted, and the complete icing and melting process was recorded.

(4) The inclination angle of the stay cable sleeve: The previous research data found that the ice thickness of the stay cable decreases with the increase in the inclination angle of the stay cable. Therefore, to make the network model more robust, the scaffold inclination angle was adjusted to 30°, 45°, and 60°, and the stay cable sleeve was placed according to the adjusted angle.

The experimental conditions are shown in Table 1.

Table 1. Experimental conditions of stay cable icing.

Group Number	Inclination Angle (°)	Ambient Temperature (°C)	Cooling Time (h)	Wind Velocity (m/s)
1	30	−4	3	2
2	30	−8	3	2
3	45	−4	3	2
4	45	−8	3	2
5	60	−4	3	2
6	60	−8	3	2

2.1.3. Experimental Steps of Stay Cable Icing

(1) Before the experiment, the spray water was purified to prevent clogging the nozzle. Secondly, the spray water temperature was reduced to 0.5 °C.
(2) The stay cable sheath was arranged under the nozzle. After the inclination angle of the scaffold was adjusted to 30°, 45°, and 60°, the stay cable sleeve was placed according to the adjusted angle, as shown in Figure 3.

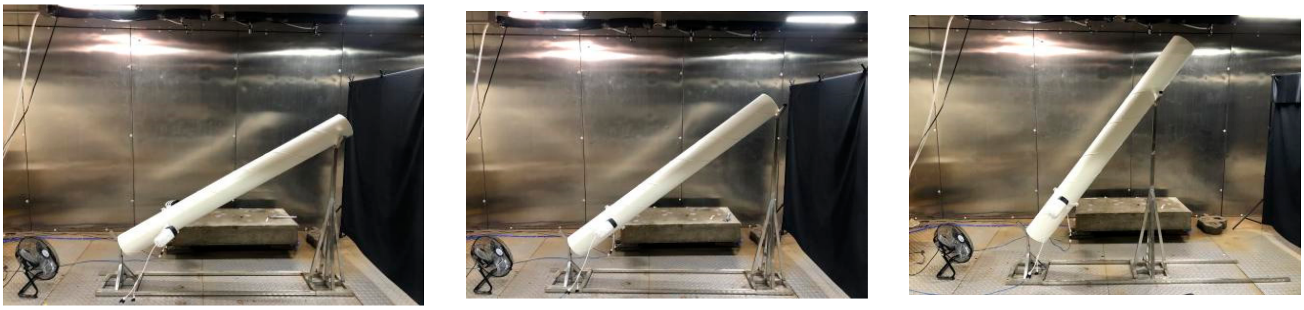

(**a**) (**b**) (**c**)

Figure 3. Icing experiment of inclined angle cable. (**a**) 30° incline angle, (**b**) 45° incline angle, (**c**) 60° incline angle.

(3) The constant temperature and humidity laboratory refrigeration was activated to maintain the indoor temperature constant at −8°C and −4 °C, and the camera was turned on.
(4) The rainfall device simulated rainfall with a spray flow rate set to 3 L per minute. The water temperature in the spray was 0.5 degrees Celsius. Simultaneously, the fan was turned on as required.
(5) The spraying was stopped after three hours, the cooling process was halted, and the temperature was adjusted to 2 degrees Celsius. This temperature was maintained until all the ice had completely melted, while the entire freezing and melting process was recorded using a camera.
(6) The inclined tension cables were dried to prepare them for the next set of experiments.

2.2. Data Processing

After the cable icing experiment was complete, the cable icing video captured by the camera was frame-by-frame clipped into a picture. However, the original icing images needed to be bigger, and their direct use for deep learning would significantly increase the time required to train and use the network model. On the other hand, reducing the size of the original image would lead to the loss of many detailed features, thereby reducing the number of features learned by the network model and would ultimately lead to a decline in the performance of the network model. To solve these problems, the method adopted in this paper cut the original cable icing image. When cropping, if the image is cropped to 0.5 to 1 times the size of the original image, unnecessary background can be effectively removed, and both ice cover and ice edges can be fully captured in the image. This not only reduces the size of the icing images but also enhances the diversity of the data set, aiding the model in learning more features and thereby improving the performance of the neural network model, as shown in Figure 4.

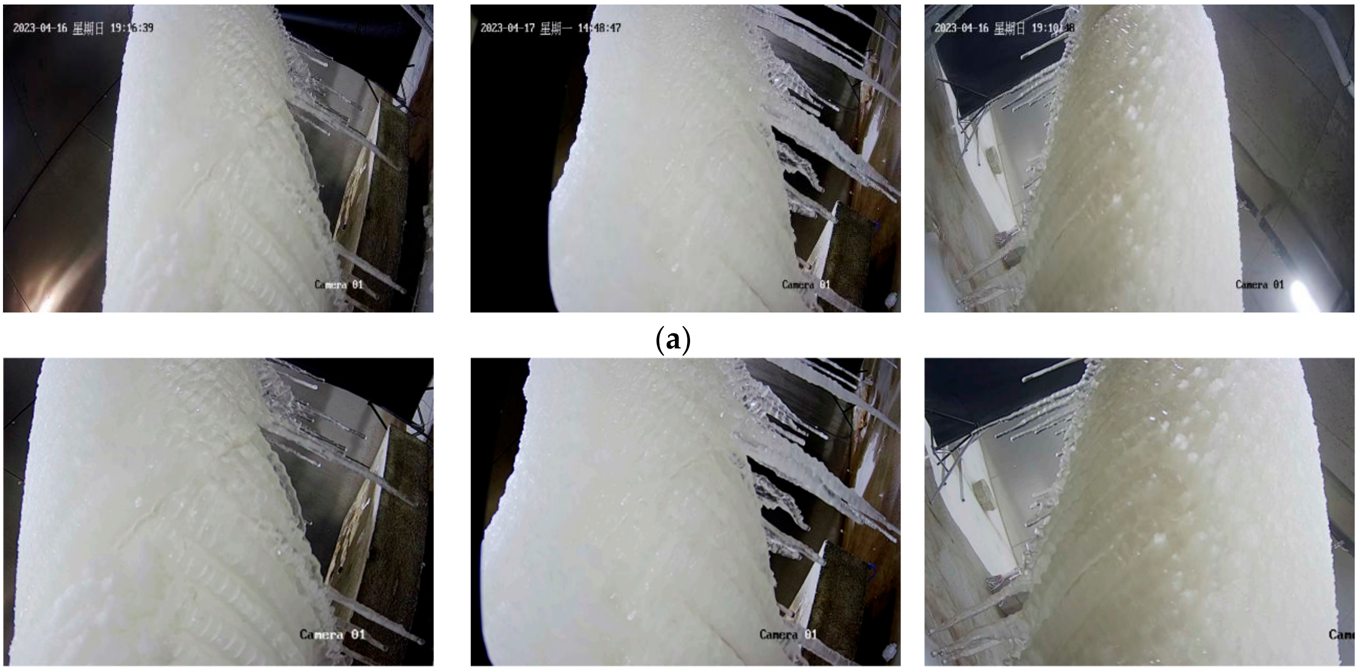

(**a**)

(**b**)

Figure 4. Examples of icing images. (**a**) Original image, (**b**) Clipped image.

2.3. Data Enhancement

Deep learning requires sufficient data to complete the training process. Increasing the data set's size is conducive to improving segmentation accuracy. In this study, image-flipping technology was used to expand the existing data, and the original cable icing image was processed horizontally and vertically to obtain a new image. The processed image is shown in Figure 5. This method can effectively increase the diversity of data sets and improve the network model's robustness to avoid over-fitting.

(**a**) (**b**) (**c**)

Figure 5. Image enhancement. (**a**) Original image, (**b**) Horizontal flip image, (**c**) Vertical flip image.

2.4. Image Classification Data Labels

At present, the stay cable deicing robot mainly uses impact deicing [1] and rotary deicing for deicing. With the increase in the icing amount, the deicing strength must also improve accordingly. Therefore, the influence of the surface ice and icicles on deicing should consider classification. However, a unified classification standard for the severity of cable icing must be improved.

This study used a method to calculate the pixel area and comprehensive icing state of cable icing through the U-Net model. The degree of cable icing was divided into three levels: zero level, first level, and second level, as shown in Table 2. Equation (1) calculates the area of pixels in the red and green channels.

$$S = S_{\text{icicle}} + S_{\text{surface ice}} \quad (1)$$

Table 2. Classification for the cable icing.

Level of Icing Degree	Icing Condition	Icing Pixel Area/mm²
zero level	no obvious icing	S = 0
first level	icing in some areas	0 < S < 100,000
second level	icing in all areas	S > 100,000

s_{icicle} represents the pixel area of the icicles after segmentation, $S_{surface\ ice}$ represents the pixel area of the icing after segmentation, and S represents the pixel area of the icing.

Take the cable-stayed sleeve with a diameter of 20 cm as an example. Image observation shows that when S is about 100,000 mm^2, the surface ice initially wraps the cable-stayed sleeve, and there is a small number of icicles. Therefore, 100,000 mm^2 is taken as the critical point. Considering the current icing condition and the area of icing pixels, the icing degree of the cable is divided into different grades, as shown in Figures 6–8. Compared with the method of only using the icing pixel area to quantify the icing degree of stay cables, this method has a better generalization ability.

(**a**) (**b**)

Figure 6. Zero level. (**a**) No obvious icing, (**b**) S = 0 mm².

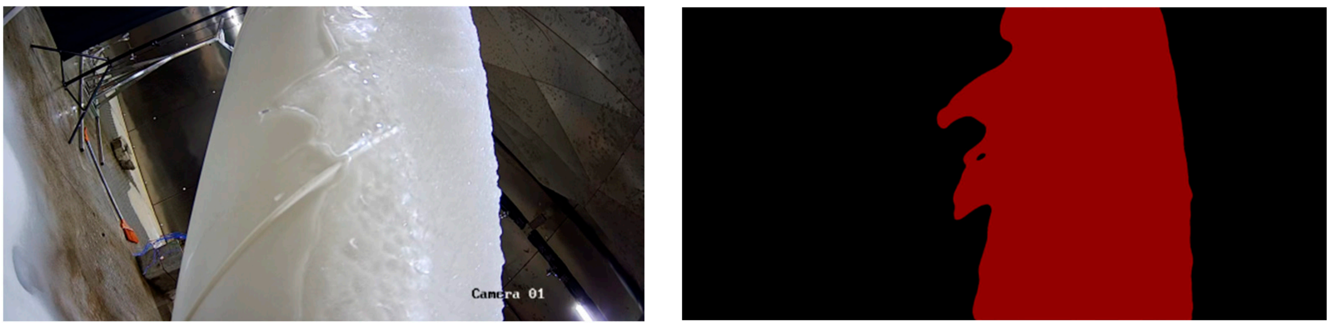

(**a**) (**b**)

Figure 7. First level. (**a**) Icing in some areas, (**b**) S = 65,391 mm².

(a) **(b)**

Figure 8. Second level. (**a**) Icing in all areas, (**b**) S = 157,006 mm².

3. Two-Stage Model

The method proposed in this paper aims to identify the location and degree of icing in the icing images of stay cables. An icing recognition model using semantic segmentation and image classification is proposed. The model transforms icing detection into a two-stage detection problem. Firstly, the semantic segmentation method is used to locate the icing position, and then the image classification method is used to rate the icing degree.

3.1. The First-Stage Model: U-Net

U-Net is a semantic segmentation network based on FCN, and its network structure is similar to that of FCN. The input of the network is 512 × 512 three-channel images. The network as a whole can be constructed as an encoding–decoding architecture or as a contraction path plus expansion path. Each step of the contraction path is composed of two 3 × 3 convolutions for feature extraction. Each step of the expansion path includes the up-sampling process of the feature map, which is matched and fused with the feature map from the contraction path. The network uses jump connection technology to connect the corresponding layers between the down-sampling and up-sampling parts to help the network better learn the detailed information in the input image. The network inputs the cable icing image and extracts the features through downsampling to obtain the abstract features. The down-sampling abstract features are restored by upsampling, and the segmentation result of the same size as the input image is generated; that is, the cable icing mask and the segmented surface ice and icicles can be used as the basis for the cable icing positioning, as shown in Figure 9.

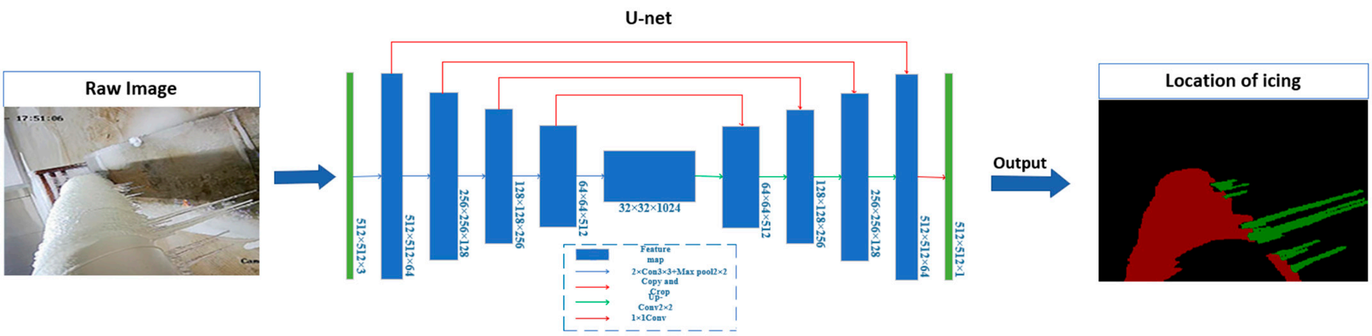

Figure 9. The network structure of U-Net.

3.2. The Second-Stage Model: ResNet50

The mask image of the stay cable icing is classified because with the increase in the neural network, there would be problems such as gradient disappearance and degradation, which makes the model difficult to train and the error rate increases. The network model, including the residual structure, avoids this problem to a large extent. Therefore, this paper chose the ResNet50 model with residual structure. ResNet50 uses a jump connection to connect the input and output ends directly. The jump connection structure is shown in Figure 10. Suppose H (x) is the output and x is the input; then H (X) = F (X) + X. The skip connection does not increase the amount of calculations, which effectively solves the problem of performance degradation caused by network deepening. The ResNet50 network is divided into six parts: stage 1 is the input module, stages 2 to 5 are the residual modules, and stage 6 is the output module. It consists of 49 convolutional layers and one fully connected layer. The network structure is shown in Figure 11.

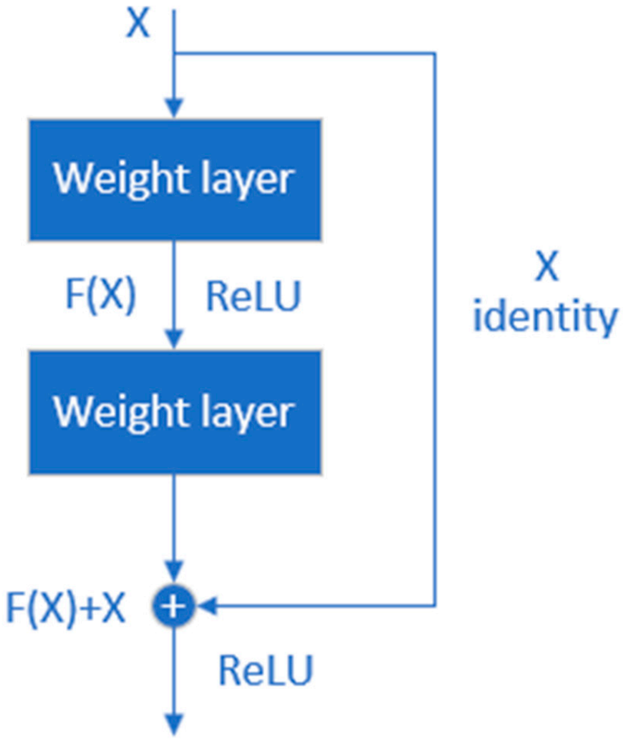

Figure 10. Jump connection structure diagram.

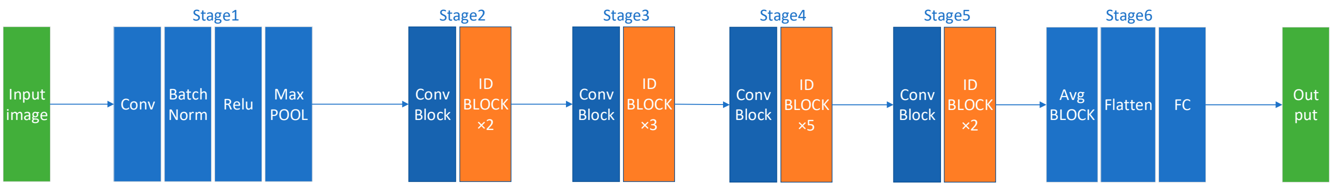

Figure 11. The network structure of ResNet50.

The ResNet50 network input module comprises CONV (convolution layer) and MAX POOL (maximum pooling layer). The Relu activation function and batch normalization layer are used in the middle to improve the network fitting ability. The four residual modules include two residual structures, CONV Block and Identity Block. The dimension of the output of the CONV Block is different from the dimension of the input, which can be used to change the network dimension. The output dimension of the Identity Block is the same as the input dimension, which deepens the network through a series connection. The output module downsamples the features through the Avg POOL average pooling layer and then changes the feature vector to batch size $\times$ 2048 through the Flatten layer. Finally, the fully connected layer is input, and the Softmax classifier outputs the corresponding current cable icing degree level.

3.3. The Stay Cable Icing Recognition Framework

In this study, the U-Net network and ResNet50 network were cascaded to identify the ice layer and icicles on the cable's surface on the cable's ice image, as shown in Figure 12. In the first stage, the original image was input into the U-Net semantic segmentation network, and the semantic segmentation was used to locate the icing area. This identified the background, icicle, and icing. In the second stage, the two-channel mask generated by semantic segmentation was input into the ResNet50 image classification network, and the output was the current icing level. The final output of this method consists of two parts: the position of the cable icicles and the surface ice, and the current icing level.

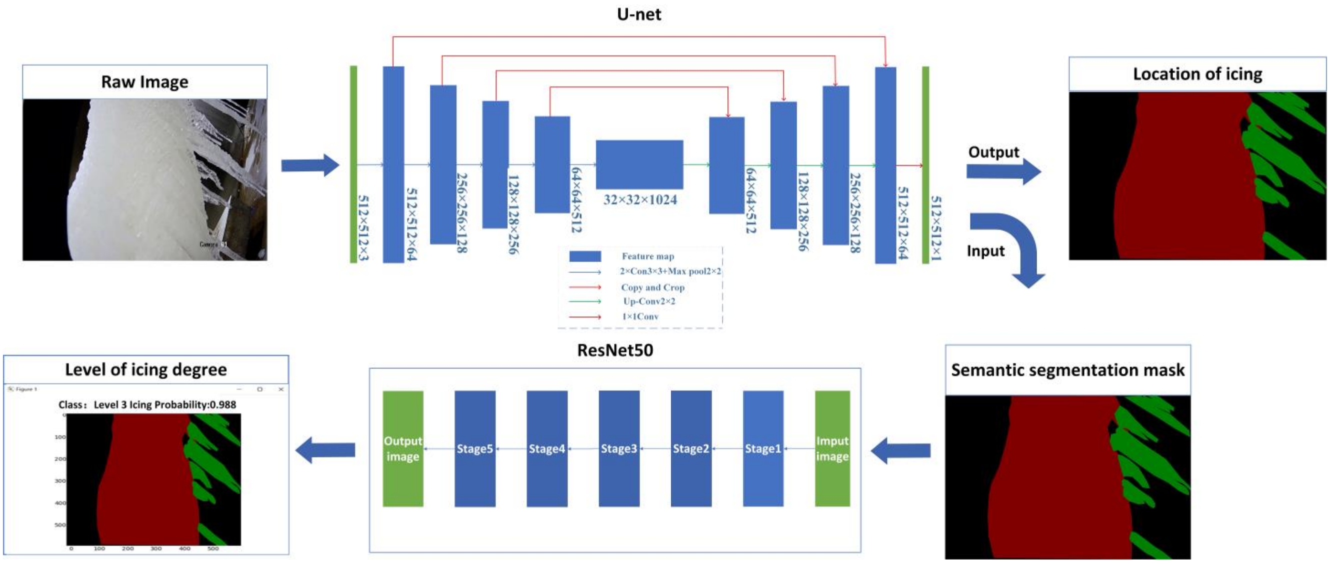

Figure 12. The stay cable icing recognition framework.

4. Experiment

This section verifies the effectiveness of this method through some experiments. Firstly, the structure and calculation source of the training set and verification set of the data set used in the cable icing identification process is described. Then, according to the evaluation index, the method's accuracy in this paper is quantitatively analyzed. Through the comparative experiments of SegNet, DeepLab, and PSPNet models, the scientificity of using U-Net to segment iced images of stay cables is verified. Then, the classification networks AlexNet, VGG16, and GoogleNet are compared with the method ResNet50 used in this paper to verify the feasibility of the two-stage deep learning icing recognition method in this paper.

4.1. Experiment Description

4.1.1. Data and Computation Source

A total of 500 original images were taken by the camera (Hikvision DS-IPC-B12V2-1), and the original image size was 1920 × 1080 pixels. First, the original image was cut manually. Then, the number of images in the data set increased to 1500 through horizontal flipping, vertical flipping, and expansion. Finally, the labelme software marked the surface ice and icicles to generate a mask map. Manually labelled images were used as a benchmark to evaluate accuracy. The method was divided into two stages. In the first stage, 1500 preprocessed images were divided into training sets and test sets according to 8:2. The training set of the second stage included 1500 mask images of U-Net, divided into training sets according to 8:2, as shown in Table 3.

Table 3. Quantity distribution of ResNet50 data set.

Level of Icing Degree	Data Set	Train	Test
Zero level	93	74	19
First level	521	416	105
Second level	886	708	178

The hardware configuration used in this research for training and testing is as follows: AMD Ryzen7 5800 H (3.20 GHz), 16 GB memory, NVIDIA GeForce RTX3060, CUDA11.6, and Pytorch1.2.0. In order to avoid the impact of hyperparameters on the experimental results, the hyperparameters of each network were configured uniformly. After trial and error, the hyperparameters were determined: learning rate 1×10^{-4}, number of epochs 300, number of iterations in each epoch 90, batch size 5, and optimizer Adam.

4.1.2. Evaluation Indicators

In order to verify the effectiveness of the proposed method based on the comparison between the prediction map and the label map, the confusion matrix was used to evaluate the model's performance. The confusion matrix evaluation model is a distinguishing method. TP represents the true positive sample, and the model also predicts the number of positive samples; FP represents the number of true negative samples, but the model predicts the number of positive samples; FN represents the true positive sample, but the model predicts the number of negative samples; TN represents the true negative sample, and the model also predicts the number of negative samples. Table 4 shows the construction method of the confusion matrix. This experiment involved the segmentation of icicles and surface ice and the estimation of icing degree level. Therefore, five indicators were applied in this experiment, namely, accuracy (A), recall (R), precision (P), F1 value, and intersection over union (IoU), to evaluate. The accuracy of the icing level estimation is evaluated by accuracy (A).

Table 4. Confusion matrix construction method.

True/Forecast	Icicles	Surface Ice	No Icing
Icicles	TP	FN	FN
Surface ice	FP	TP	TN
No icing	FP	FP	TP

Accuracy is the percentage of correctly identified pixels relative to all pixels, indicating the proportion of the model's correct prediction to the total prediction value, as shown in Equation (2).

$$accuracy = \frac{TP + TN}{TP + TN + FN + FP} \tag{2}$$

The proportion of the part of the accuracy rate that is positive, and indeed positive in all classifiers, is considered to be positive, and indicates the proportion of the model in all positive results in the prediction graph to predict correctly, as shown in Equation (3).

$$pision = \frac{TP}{TP + FP} \tag{3}$$

The recall rate refers to the proportion of the part of the classifier that is considered to be a positive class and is indeed a positive class in the proportion of all classifiers that are considered to be a positive class, indicating that the true value is a positive example of all the results. The model predicts the correct proportion, as shown in Equation (4).

$$recall = \frac{TP}{TP + FN} \tag{4}$$

The F1 value combines the precision rate and the recall rate, as shown in Equation (5).

$$F1 = 2 \times \frac{precision \times recall}{precison + recall} \tag{5}$$

IoU is a standard metric for measuring the accuracy of image segmentation algorithms. The larger the IoU value, the higher the segmentation accuracy. The method for calculating IoU is to divide the intersection of the predicted region and the actual region by the union of the predicted region and the actual region, as shown in Equation (6).

$$IOU = \frac{TP}{TP + FN + FP} \tag{6}$$

4.2. Experimental Results and Analysis

4.2.1. Comparison of Segmentation Models

Several popular semantic segmentation networks were evaluated and compared with the U-Net architecture for the purpose of image segmentation. The goal was to retain the characteristics of icing and complete the identification of the icing area. It is required that the model has strong robustness to icing segmentation. Table 5 lists the real label map of the original image of cable icing. Correspondingly, under the same training conditions, SegNet [22], DeepLab [23], and PSPNet [24] models have the best segmentation map for the icicles and surface ice layer.

Table 5. Segmentation results of ice-covered stay cables (%).

Model	Category	Accuracy	IoU	Precision	Recall	F1
DeepLab	background	93.48	87.04	92.97	93.17	93.07
	surface ice	96.09	91.84	96.09	95.40	95.74
	icicles	96.29	46.50	61.97	65.07	63.48
PSPNet	background	93.15	86.51	92.08	93.46	92.77
	surface ice	95.63	91.31	95.45	95.46	95.46
	icicles	96.40	43.75	65.93	56.54	60.87
SegNet	background	92.76	85.85	91.40	93.40	92.39
	surface ice	95.10	90.27	95.22	94.55	94.88
	icicles	96.28	42.54	64.52	55.53	59.69
U-Net	background	**95.41**	**90.62**	**95.80**	**94.37**	**95.08**
	surface ice	**97.08**	**94.11**	**96.95**	**96.98**	**96.97**
	icicles	**97.48**	**61.58**	**71.59**	**81.49**	**76.22**

In the qualitative comparison, the segmentation result map of DeepLab contained many incomplete icicles and icing, and the segmentation effect of icicles could be better. Although it could segment the large surface ice layer well, it was unsuitable for tiny icicles; the holes and noise in the ice segmentation results of the PSPNet were not wholly compared with the real label, and the edge of the icicles was blurred in the detection. This incomplete segmentation feature would lead to poor performance in predicting the ice grade of the cable. SegNet and PSPNet could be stronger in the segmentation of icing and icicles, and there are severe drawbacks to insufficient segmentation ability. Compared with the above three popular networks, the U-Net image segmentation ability used in this paper was the best, manifested in the minor error segmentation content (red and green marks in the graph). In Table 6, the original image of the right side camera of the example had a large icicles area, which is an excellent test for the model segmentation ability. The prediction results show that U-Net still had good segmentation ability for such samples. Therefore, U-Net makes up for the over-segmentation of DeepLab and the under-segmentation of SegNet and PSPNet.

Table 6. Qualitative comparison of ice segmentation tasks for stay cables.

Camera Perspective	Origin	Ground Truth	SegNet	DeepLab	PSPNet	U-Net
Left camera	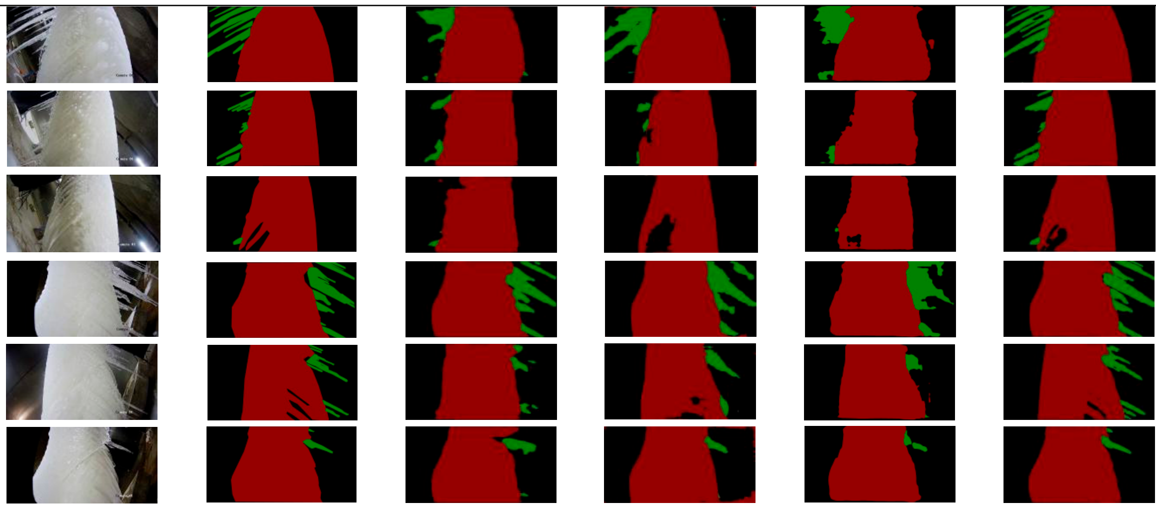					
Right camera						

In addition to visual comparison, Table 5 shows the performance of each model on the test set in terms of background category, surface ice category, and icicles category in quantitative comparison. We used Accuracy, IoU, Precision, Recall, and F1 value evaluation indicators to evaluate U-Net over DeepLab, PSPNet and SegNet models.

Regarding segmentation accuracy, the U-Net used in this paper achieved better performance parameters than the comparison model. The Accuracy, IoU, Precision, Recall, and F1 values of U-Net for the surface ice category were 97.08%, 94.11%, 96.95%, 96.98%, and 96.97%, respectively. The Accuracy, IoU, Precision, Recall, and F1 values of the icicles category were 97.48%, 61.58%, 71.59%, 81.49%, and 76.22%, respectively. This is due to the U-Net's U-shaped encoding–decoding structure, which has rich feature representation capabilities. It preserves the context information of different scales by gradually upsampling and skipping the feature map so that the network can better capture the details and context information of the target. By calculating the MIOU changes, U-Net converged to 82.10%, SegNet converged to 72.89%, PSPNet converged to 73.85%, and DeepLab converged to 75.13%. U-Net was 6.97% higher than the DeepLab model with poor performance and 9.21% higher than the SegNet model with relatively poor performance. Therefore, it was well-suited to the icing segmentation task of stay cables regarding all-around performance.

Based on the fact that only surface ice pixels and icicles pixels are used to judge the icing level of the cable, Figure 13 shows the F1 value and intersection ratio of each model on the surface ice category and the icicles category. For the surface ice category, the U-Net used in this paper was at least 1.21% and 2.27% higher than the DeepLab, PSPNet, and SegNet models in the F1 value and IOU, and the segmentation accuracy of the comparison model on the icicles category was not high. However, the U-Net was at least 12.74% and 15.08% higher than the DeepLab, PSPNet, and SegNet models in the F1 value and IOU. F1 score is a metric that comprehensively considers both precision and recall. A higher F1 score indicates better model performance and predictive accuracy. IoU (Intersection over Union), on the other hand, is a metric used to measure the degree of overlap between predicted bounding boxes or segmentation results and ground truth bounding boxes or segmentation results in object detection or image segmentation tasks. In this study, since joint operation was required, the accuracy of the first stage directly affected the operation of the second stage, so the mask that used the U-Net model to calculate the icing area was better than the other networks.

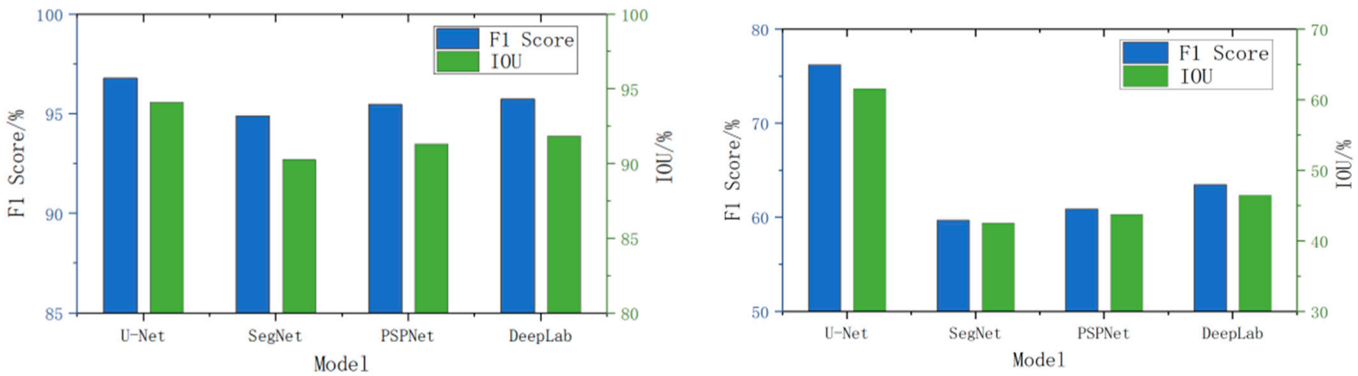

(**a**) (**b**) Icicles

Figure 13. The performance of the segmentation model on the surface ice layer category and the icicles category. (**a**) Surface ice segmentation perfomance, (**b**) Icicles segmentation perfomance.

4.2.2. Icing Severity Classification

The problem of classifying the icing degree of stay cables was solved by image classification. For this reason, the mask generated by the icing segmentation of stay cables was used as the input of image classification, and the output was the current icing degree grade. In the cable icing data set, the F1 value and IOU of the U-Net model were better than the other models, and the comprehensive evaluation index was the highest.

As shown in Table 7, the mask after image segmentation by U-Net was input into several current popular image classification networks. Among them, ResNet50 was used as a classifier to achieve the highest accuracy of 95.71%, 9.39% higher than VGG16, which had the worst relative accuracy. The second stage used the ResNet50 model as a classifier superior to other classification networks.

Table 7. Comparison of classification accuracies of stay cable icing masks using different methods.

Model	A/%
U-Net + VGG16 (Simonyan, 2014)	86.32
U-Net + AlexNet (Krizhevsky et al., 2012)	88.95
U-Net + ResNet50 (He et al., 2016)	95.71
U-Net + GoogleNet (Szegedy et al., 2015)	89.43

5. Conclusions

In this paper, a two-stage deep learning framework based on cable icing images was designed. In the first stage, U-Net was used to segment icicles and icing accurately. In the second stage, ResNet50 was employed to classify the segmentation results and determine the icing level. This novel approach allowed for the utilization of image information to effectively locate the current icing area and classify the icing level with a reasonable degree of accuracy. The MIoU of U-Net for icing feature segmentation reached 82.10%, and the average accuracy was 96.66%. ResNet50 classified the icing degree grade, and the average accuracy was 95.71%. Compared to the method of only using the icing pixel area to quantify the icing degree grade of the stay cable, this method has a better generalization ability and a more comprehensive application range. This research not only provides a theoretical basis for the study of two-stage deep learning models but also provides technical support for the accurate classification of the icing degree of stay cables and the accurate positioning of the robot.

Author Contributions: Z.Y. conceived, designed, and analyzed the test results; F.X. provided ideas and modification suggestions; F.X. wrote the manuscript; Y.P. used software; Z.C. performed project administration; E.H. and G.Z. participated in the processing of some data; C.Z. Investigation.

All authors have made equal contributions to the revision of the paper. All authors have read and agreed to the published version of the manuscript.

Funding: This research was funded by the key projects of Hubei Provincial Department of Education (No. D20211403) and The Key Research amd Development Program of Hubei Province (No. 2023BCB116).

Institutional Review Board Statement: Not applicable.

Informed Consent Statement: We declare that all authors have given informed consent.

Data Availability Statement: The raw data supporting the conclusions of this article will be made available by the authors on request.

Conflicts of Interest: The authors declare no conflicts of interest.

References

1. Li, S.; Wu, T.; Huang, T.; Chen, Z. Aerodynamic Stability of Iced Stay Cables on Cable-Stayed Bridge. *Wind. Struct.* **2016**, *23*, 253–273. [CrossRef]
2. Liu, Q.; Han, Y.; Fan, X. Research on Hot Air Ice Melt System for Cable Sheaths of Er'qi Yangtze River Bridge. *E3S Web Conf.* **2021**, *237*, 02006. [CrossRef]
3. Zicun, H.; He, K.; Xu, Y.G.; Fang, H.; Zuo, Q.; Li, Z. Design and Research on Impact Deicing Mechanism of Cable Climbing Robot. In Proceedings of the Design and Research on Impact Deicing Mechanism of Cable Climbing Robot 2021, Shanghai, China, 8–10 January 2021. [CrossRef]
4. Kumpf, J.; Helmicki, A.; Nims, D.K.; Hunt, V.; Agrawal, S. Automated Ice Inference and Monitoring on the Veterans' Glass City Skyway Bridge. *J. Bridge Eng.* **2012**, *17*, 975–978. [CrossRef]
5. Roldsgaard, J.H.; Kiremidjian, A.S.; Georgakis, C.; Faber, M.H. Preliminary Probabilistic Prediction of Ice/Snow Accretion on Stay Cables Based on Meteorological Variables. In Proceedings of the 11th International Conference on Structural Safety & Reliability Conference, New York, NY, USA, 16–20 June 2014; pp. 5531–5538. [CrossRef]
6. Andre, J.; Kiremidjian, A.S.; Georgakis, C. Statistical Modeling of Time Series for Ice Accretion Detection on Bridge Cables. *J. Cold Reg. Eng.* **2018**, *32*, 04018004. [CrossRef]
7. Xiong, L.; Zhang, J.; Zheng, X.; Wang, Y. Context Transformer and Adaptive Method with Visual Transformer for Robust Facial Expression Recognition. *Appl. Sci.* **2024**, *14*, 1535. [CrossRef]
8. Wang, B.; Fuqi, M.; Ge, L.; Ma, H.; Wang, H.; Mohamed, M.A. Icing-EdgeNet: A Pruning Lightweight Edge Intelligent Method of Discriminative Driving Channel for Ice Thickness of Transmission Lines. *IEEE Trans. Instrum. Meas.* **2021**, *70*, 1–12. [CrossRef]
9. Bindu, N.P.; Sastry, P.N. Automated Brain Tumor Detection and Segmentation Using Modified UNet and ResNet Model. *Soft Comput.* **2023**, *27*, 9179–9189. [CrossRef]
10. Fischl, B.; Salat, D.H.; Busa, E.; Albert, M.; Dieterich, M.; Haselgrove, C.; van der Kouwe, A.; Killiany, R.; Kennedy, D.; Klaveness, S.; et al. Whole Brain Segmentation: Automated Labeling of Neuroanatomical Structures in the Human Brain. *Neuron* **2002**, *33*, 341–355. [CrossRef] [PubMed]
11. Ronneberger, O.; Fischer, P.; Brox, T. U-Net: Convolutional Networks for Biomedical Image Segmentation. In *Proceedings of the Medical Image Computing and Computer-Assisted Intervention–MICCAI*; Springer: Berlin/Heidelberg, Germany, 2015; pp. 234–241.
12. Zhou, Z.; Rahman Siddiquee, M.M.; Tajbakhsh, N.; Liang, J. UNet++: A Nested U-Net Architecture for Medical Image Segmentation. In *Proceedings of the Deep Learning in Medical Image Analysis and Multimodal Learning for Clinical Decision Support*; Springer: Cham, Switzerland, 2018.
13. Bahadure, N.B.; Ray, A.K.; Thethi, H.P. Comparative Approach of MRI-Based Brain Tumor Segmentation and Classification Using Genetic Algorithm. *J. Digit. Imaging* **2018**, *31*, 477–489. [CrossRef] [PubMed]
14. Long, J.; Shelhamer, E.; Darrell, T. Fully convolutional networks for semantic segmentation. In Proceedings of the IEEE Conference on Computer Vision and Pattern Recognition, (CVPR), Boston, MA, USA, 7–12 June 2015; pp. 3431–3440. [CrossRef]
15. Guo, Q.; Xiao, J.; Hu, X. New Keypoint Matching Method Using Local Convolutional Features for Power Transmission Line Icing Monitoring. *Sensors* **2018**, *18*, 698. [CrossRef] [PubMed]
16. Pan, G.; Fu, L.; Yu, R.; Muresan, M. Evaluation of Alternative Pre-Trained Convolutional Neural Networks for Winter Road Surface Condition Monitoring. In Proceedings of the 2019 5th International Conference on Transportation Information and Safety (ICTIS), Liverpool, UK, 14–17 July 2019.
17. Veerakumar, R.; Gao, L.; Liu, Y.; Hu, H. Dynamic Ice Accretion Process and Its Effects on the Aerodynamic Drag Characteristics of a Power Transmission Cable Model. *Cold Reg. Sci. Technol.* **2020**, *169*, 102908. [CrossRef]
18. Sampedro, C.; Rodriguez-Vazquez, J.; Rodriguez-Ramos, A.; Carrio, A.; Campoy, P. Deep Learning-Based System for Automatic Recognition and Diagnosis of Electrical Insulator Strings. *IEEE Access* **2019**, *7*, 101283–101308. [CrossRef]
19. Wang, C.-S.; Du, P.; Wu, H.; Li, J.; Zhao, C.; Zhu, H. A Cucumber Leaf Disease Severity Classification Method Based on the Fusion of DeepLabV3+ and U-Net. *Comput. Electron. Agric.* **2021**, *189*, 106373. [CrossRef]
20. He, K.; Zhang, X.; Ren, S.; Sun, J. Deep residual learning for image recognition. In Proceedings of the IEEE Computer Society Conference on Computer Vision and Pattern Recognition (CVPR), Las Vegas, NV, USA, 27–30 June 2016; pp. 770–778. [CrossRef]

21. Liu, T.; Tao, D.; Song, M.; Maybank, S.J. Algorithm-Dependent Generalization Bounds for Multi-Task Learning. *IEEE Trans. Pattern Anal. Mach. Intell.* **2017**, *39*, 227–241. [CrossRef] [PubMed]
22. Badrinarayanan, V.; Kendall, A.; Cipolla, R. SegNet: A Deep Convolutional Encoder-Decoder Architecture for Image Segmentation. *IEEE Trans. Pattern Anal. Mach. Intell.* **2017**, *39*, 2481–2495. [CrossRef] [PubMed]
23. Chen, L.-C.; Papandreou, G.; Kokkinos, I.; Murphy, K.; Yuille, A.L. DeepLab: Semantic Image Segmentation with Deep Convolutional Nets, Atrous Convolution, and Fully Connected CRFs. *IEEE Trans. Pattern Anal. Mach. Intell.* **2018**, *40*, 834–848. [CrossRef]
24. Zhao, H.; Shi, J.; Qi, X. Pyramid Scene Parsing Network. *Proc. IEEE Conf. Comput. Vis. Pattern Recognit.* **2017**, *2017*, 2881–2890.